

Spectrally Resolved Dynamics of Synthesized CdSe/ZnS Quantum Dot/Silica Nanocrystals for Photonic Down-Shifting Applications

Bahareh Sadeghimakki, *Member, IEEE*, Navid M. S. Jahed, *Student Member, IEEE*,
and Siva Sivoththaman, *Senior Member, IEEE*

Abstract—Photonic structures capable of luminescence down-shifting (LDS) have strong application potential in several areas of optoelectronics. Such structures can be formed by overcoating quantum dots (QDs) with integrable, transparent layers. In this paper, silica was grown on CdSe/ZnS QDs to form QD/silica nanocrystals (NCs) in a microemulsion synthesis process. The synthesized structures were structurally and optically characterized to understand the growth mechanism, luminescence properties, and the influence of process parameters on excitonic decay and lifetime. Process conditions were established to have single QDs at the centers of the silica particles. The effects of temperature, excitation duration, size of QDs, and type of ligands on decay dynamics were established. Temperature- and time-resolved excitonic decay study of QD/silica NCs suggested carrier-trapping at the QD/silica interface and the exciton-phonon coupling to be the two main nonradiative processes limiting the luminescence efficiency. The synthesized NCs displayed intense photoluminescence (PL) with slight decrease in lifetime. The PL efficiency of the NCs improved for longer illumination. The NC structures that safely embed QDs in transparent medium are good candidates for LDS applications in photovoltaic, imaging, and detection devices.

Index Terms—CdSe/ZnS quantum dot (QD), excitonic decay, ligand exchange, luminescence down-shifting (LDS), photoluminescence (PL), QD/silica nanocrystals (NCs), synthesis.

I. INTRODUCTION

PHOTONIC and electronic properties of quantum dots (QDs) are drawing tremendous attention for a broad range of applications [1]–[3]. The luminescence quantum efficiency (LQE) of QDs is a key parameter determining the performance in devices such as photovoltaic (PV) cells, photo detectors, light emitters, imagers, etc. In addition to high LQE, the QDs should preferably possess a broad absorption band, size-tunability of emission wavelengths, and narrow emission band. Due to high surface-to-volume ratios in QDs, LQE is limited by nonradiative processes associated with surface trap states. Employing core/shell QD structures with a wider bandgap shell material improves LQE by confinement of excitons.

Manuscript received October 15, 2013; revised March 5, 2014; accepted January 27, 2014. Date of publication May 16, 2014; date of current version July 2, 2014. The review of this paper was arranged by Associate Editor E. T. Yu.

The authors are with the Centre for Advanced Photovoltaic Devices and Systems, Department of Electrical and Computer Engineering, University of Waterloo, Waterloo, ON N2L 3G1, Canada (e-mail: b2sadegh@uwaterloo.ca; n6mohamm@uwaterloo.ca; sivoththaman@uwaterloo.ca).

Color versions of one or more of the figures in this paper are available online at <http://ieeexplore.ieee.org>

Digital Object Identifier 10.1109/TNANO.2014.2324973

Luminescence down-shifting (LDS), in which a high energy photon is converted into a low energy photon, shows great promise for application in PV. Power conversion efficiency of PV cells that have poor spectral response to high energy photons can be enhanced by LDS [4]. QDs, due to their tunable properties, offer unique opportunities for LDS. Several QD-based approaches have been proposed for PV cells and modules [5]–[7]. Other materials that have been considered for LDS in PV devices include fluorescent rare earth ions [8], phosphor coatings [9], and organic dyes [10]. In addition to PV, QD-based LDS has been proposed for imaging applications [11], [12] to enhance the performance of multispectral imaging devices with added UV capability. In display applications, QD down conversion can be used with light emitting diode backlit liquid crystal displays [13]. Another area where LDS using QDs can be used is sensitizing short wavelength infrared detectors to UV light [14].

Achieving a high LQE in the QDs is key to successful LDS in the earlier applications. To date, experimental efforts in down-shifting using Si nanostructures [15] and QDs [5], [16], [17] embedded in transparent matrices have shown limited success. While core/shell CdSe/ZnS QDs have been good candidate for LDS, their low absorption coefficient limits the LQE. Embedding QDs in a host matrix and nonuniform dispersion due to agglomeration are some other practical factors limiting the LQE.

Synthesis of QD/silica nanocrystal (NC) structures with a silica outer shell can provide better passivation and improve LQE. Furthermore, applying self-assembly processes [18] and embedment processes in photonic transparent layers [19] can lead to structures with enhanced down-shifting and absorption properties. Photonic properties of periodic arrays of QDs embedded in transparent medium can also be exploited, through enhanced scattering, to improve the absorption efficiency of the starting colloidal QDs. Also, employing synthesis processes [20] to form a thin metal layer on the QD/silica NCs will lead to realization of plasmonic structures [21]. It is also important to note that the toxicity and safety risks [22] associated with deployment of QDs can also be mitigated by the added silica shell layer.

In this paper, a microemulsion approach [23]–[29] was used to synthesize CdSe/ZnS/silica NCs. The structural and optical characterization of the synthesized NCs was carried out in order to study the silica growth mechanism, sources on nonradiative recombination, and suitability as LDS layer.

II. GROWTH OF CdSe/ZnS QD/SILICA NANOCRYSTALS

For the synthesis of QD/silica NCs, commercially available stock solutions of CdSe/ZnS (trioctylphosphine oxide TOPO-ligated QDs from American Elements: QD-530E, 550E, 610E, and Octadecylamine ODA-ligated QDs from NN-Labs: CZ610-25) were used. In order to grow the silica shell onto the QDs by microemulsion, 10 mL of cyclohexane, 1.3 mL of nonylphenol ethoxylate (NP-9), and 80 μL of tetraethyl orthosilicate (TEOS, 99.999%) were incorporated into a flask along with 400 μL of either TOPO- or ODA-ligated CdSe/ZnS solution under strong stirring. The polymerization process was initiated about 30 min after formation of the microemulsion system, by the addition of 150 μL aqueous ammonia (33 wt%) solution. After completion of the silica growth and stirring for 24 h, the solution was precipitated by adding acetone and was centrifuged to isolate the NCs from the microemulsion. The resultant CdSe/ZnS/silica NCs were washed sequentially with 1-butanol, 1-propanol, ethanol and finally water. Highly luminescent organic dispersions of the QD/silica NCs were obtained by dispersing the precipitate in methanol.

III. CHARACTERIZATION METHODS FOR THE NANOCRYSTALS

The structure, size, and morphology of the resulting NCs were studied by high-resolution transmission electron microscopy (HRTEM, FEI Titan 80-300 HB, FEI Co.), Fourier transform infrared spectroscopy (FTIR, Bruker Optics, Vertex 70), and scanning electron microscopy (SEM, FE XL 30, Philips Co.). Photoluminescence (PL) spectra and fluorescence imaging were done using a fluorescence spectrometer (Edinburgh Instruments) equipped with a confocal scanning microscope (Olympus BX 51). A 450W Xenon lamp was used as the excitation source. Upon excitation at 380 nm the emission was recorded using a cooled photomultiplier detector. The decay curves were obtained by time correlated single photon counting (TCSPC) method with nanosecond flash lamp excitation. In order to allow measurements down to 77 K, the samples were placed in a cryostat (Optistat, Oxford Instruments). The raw decay data were iteratively deconvoluted from the instrument response function (IRF) and fitted to decay functions using fluorescence analysis software technology (FAST, Edinburgh Instrument), which allowed more than four decay constants to be obtained by multiexponential and distribution tail fitting analyses, ensuring that $\chi^2 < 1.3$. Absorption spectra were recorded using a UV-vis spectrophotometer (Perkin-Elmer Lambda 1050).

IV. STRUCTURE AND MORPHOLOGY OF THE SYNTHESIZED QD/SILICA NANOCRYSTALS

In order to examine the influence of the concentration of QDs on monodispersity or multiplicity of QDs per silica particle, 400 μL TOPO-ligated QD solutions containing 6.5 nm QDs with different concentrations of 0.2, 0.8, and 1 mg/mL were used. With 0.2 mg/mL solution the dispersity was acceptable, but many silica particles without QDs appeared [see Fig. 1(a)]. On the other hand, particles with multiple QDs resulted from 1 mg/mL solution [see Fig. 1(b)]. The 0.8 mg/mL concentration

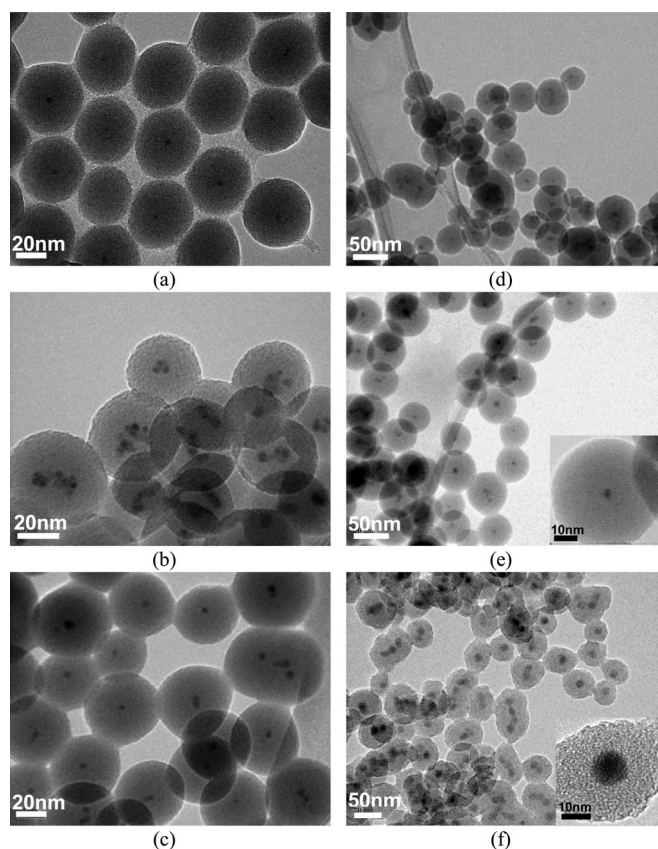


Fig. 1. TEM micrograph of core/shell CdSe/ZnS/silica NCs at (a) low (0.2 mg/mL), (b) high (1 mg/mL), and (c) optimum (0.8 mg/mL) concentration of the QDs, (d) QD/silica particles prepared with mixed 3.5 and 6.5 nm QDs, (e) QD/silica particles prepared with TOPO-stabilized QDs, and (f) ODA-stabilized QDs. Insets in (e) and (f) are HRTEM images of a single NC.

resulted in silica particles with just one QD in each as shown in Fig. 1(c). As evidenced by the TEM results the QDs were found mostly in the middle of the silica particles, indicating that the QDs act as nuclei for the silica growth. To investigate the effect of the QD size on the growth process, TOPO-ligated QDs with sizes of 3.5 and 6.5 nm were mixed and added to the solution in a separate test. A close analysis of the TEM image in Fig. 1(d) indicated that the size of the resulting NC correlates to the QD seed.

Both TOPO- and ODA-ligated QD solutions were used for the silica shell growth to study the influence of the ligands on the resulting NCs. Fig. 1(e) and (f) shows the resulting NCs after silica growth on TOPO- and ODA-ligated CdSe/ZnS QDs, respectively. QDs with ODA ligands resulted in more polydisperse silica spheres with a larger spread in the number of QDs per silica particle.

Monodisperse silica spheres in the size range of 40–70 nm were grown by controlled hydrolysis and condensation of TEOS within reverse micelles [23], [30] that provides great flexibility to form shells with desired thicknesses on QDs. From the experimental results, it has been found that the ligands, size and concentration of QDs have strong influence on the size of the resulting QD/silica NCs, and on the monodispersity/multiplicity of QDs.

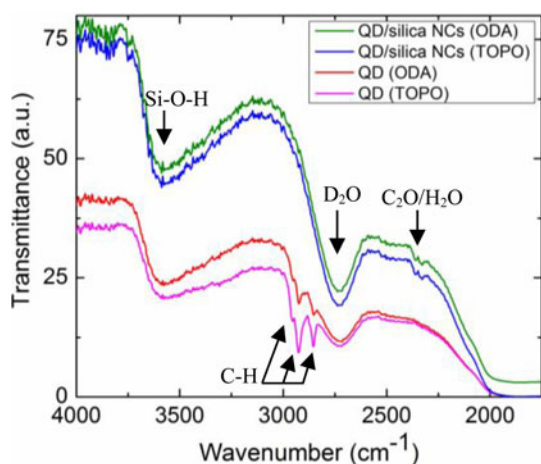


Fig. 2. FTIR spectra of CdSe/ZnS QDs with and without silica shell.

The silica growth in this paper was likely resulting from the exchange of QD hydrophobic ligands with hydroxyl-functionalized ligands (TEOS) which have a high affinity for the QD surface, enabling the transfer of the QDs to the hydrophilic interior of the micelles where silica growth takes place [23], [31]–[34].

To further investigate this hypothesis on ligand exchange, FTIR measurements [see Fig. 2] were performed on solid films of QDs with and without the silica shell. In both cases, the films were identically drop cast from colloidal solutions onto glass substrates. For both types of films peaks corresponding to adsorbed CO₂/H₂O (2334 and 2361 cm⁻¹) [35]–[38], D₂O (2733 cm⁻¹) [37], [39], and Si-OH stretching (3568 cm⁻¹) [32], [40], [41] were detected. On the other hand, peaks corresponding to C–H bonds (2851, 2920, and 2955 cm⁻¹) [35], [40], [41] were observed only in the film of QDs without silica shell. This observation seems to suggest the ligands were present only in the bare QD films. Also it can be noted in the HRTEM images of QD/silica NCs [insets of Fig. 1(e) and (f)] that no detectable transition layer was present.

V. PL SPECTRA AND FLUORESCENCE RESPONSE OF THE SYNTHESIZED QD/SILICA NANOCRYSTALS

The absorption, PL spectra and fluorescence images of the synthesized QD/silica NCs were investigated using the setup shown in Fig. 3. Since the shell growth affects the peak energy of the absorption bands, the absorption spectra in Fig. 4(a) indicate a successful growth of the silica shell on hydrophobically ligated CdSe/ZnS QDs without influencing the QD optical properties. Fig. 4(b) shows the PL spectra of NCs before and after silica shell growth for three different QD sizes of 3.5, 5.5, and 6.5 nm. The slight red shift of the PL maximum caused by the silica shell could be due to the elastic stress. Films of QD/silica were also prepared by drop casting [see Fig. 4(c)] for confocal microscopy analysis which demonstrated high fluorescence at an excitation wavelength of 380 nm. Fig. 4(d) shows the fluorescence images of QD/silica NCs for two QD sizes of 6.5 and 5.5 nm.

Analyses of the temperature-dependent PL and excitonic decay of the synthesized NCs are presented in the following sections.

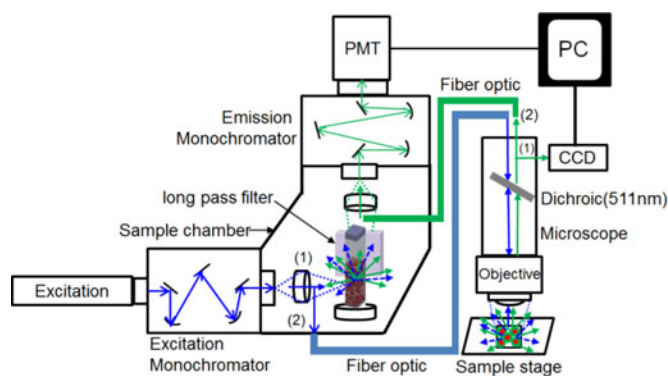


Fig. 3. Schematic diagram of the PL system (“1” and “2” represent different paths used in the measurements).

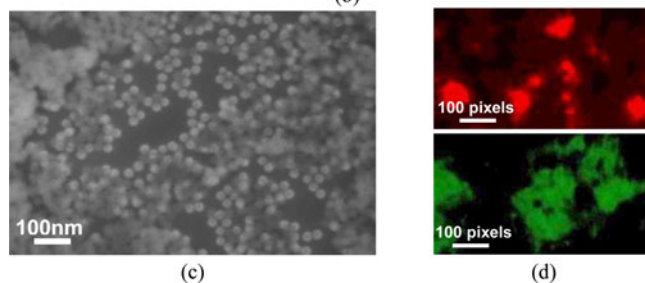
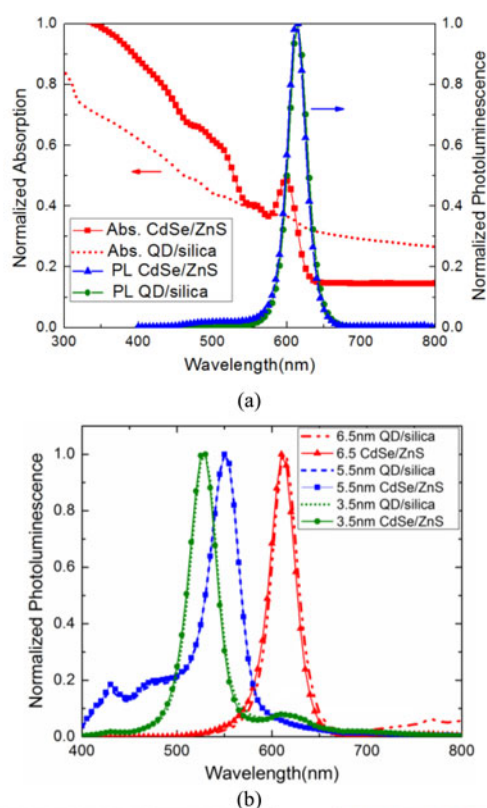


Fig. 4. (a) Normalized absorption and PL spectra of CdSe/ZnS QDs and QD/silica NCs. (b) PL correlated to QD and QD/silica NCs with different sizes; QDs = 3.5 nm (green lines), QDs = 5.5 nm (blue lines), and QDs = 6.5 nm (red lines). (c) SEM image of a film of QD/silica NCs. (d) Fluorescence image at excitation wavelength of 380 nm for QD/silica NCs with the QDs size of 6.5 nm (top) and 5.5 nm (bottom).

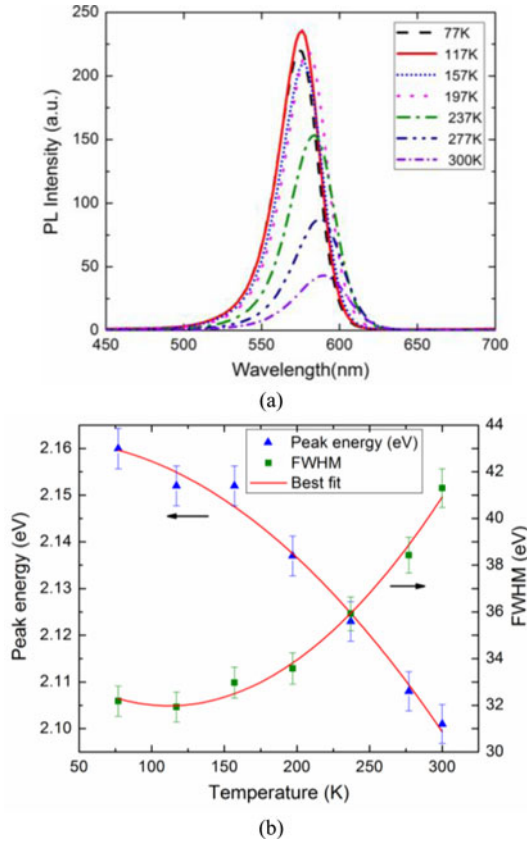


Fig. 5. (a) PL spectra of QD/silica NCs as a function of the temperature (measured at 380 nm excitation). (b) PL peak energy (blue triangles) and FWHM (green squares) as a function of the temperature. The red lines are the best-fits.

A. Temperature-Dependent PL of the QD/Silica Nanocrystals

The PL spectra of the QD/silica NCs, measured at 380 nm excitation, as a function of the temperature (T) are shown in Fig. 5(a). The increase in temperature causes decrease in the PL intensity, red shifts in emission energy, and spectra broadening. Fig. 5(b) shows the PL peak energy and the full width at half maximum (FWHM) Γ as a function of T . The peak energy, which represents the QD energy gap, shows a red shift of about 60 meV as T increases from 77 K to 300 K. The experimental data were also fitted to the Varshni relation, shown in (1), which describes the T -dependence of the PL peak energy in bulk semiconductors [42]:

$$E_g(T) = E_{g0} - \frac{\alpha T^2}{(T + \beta)}. \quad (1)$$

In (1), E_{g0} , α and β represent the energy gap at 0 K, temperature coefficient and the Debye temperature of the material, respectively. For the best-fit the values obtained were, $E_{g0} = 2.06$ eV, $\alpha = 0.4$ meV/K and $\beta = 310$ K, indicating the experimental data are close to the values known in the literature for bulk CdSe: 2.13 eV for E_{g0} , $(2.8\text{--}4.1)10^{-4}$ eV/K for α and $(181\text{--}315)$ K for β [43]. The results demonstrate the T -dependent bandgap shrinkage of the QDs causes the energy shift.

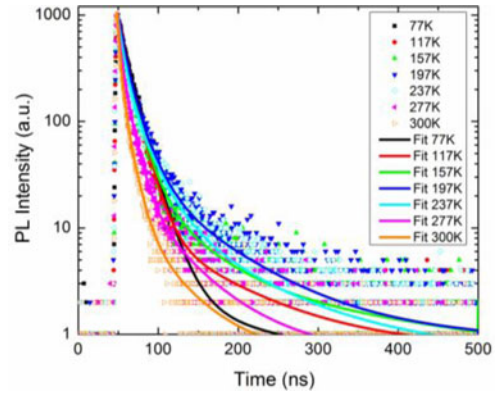


Fig. 6. Relaxation dynamics in QD/silica NCs as a function of the sample temperature. The solid lines are the best-fits.

Fig. 5(b) also shows that the FWHM (Γ) of the PL peak increases with T . The experimental data were fitted to (2), which defines the T -dependence of the excitonic peak broadening in QDs [44]:

$$\Gamma(T) = \Gamma_{inh} + \delta T + \Gamma_{LO} \left(e^{\frac{E_{LO}}{K_B T}} - 1 \right)^{-1} \quad (2)$$

In (2), Γ_{inh} is the inhomogeneous broadening and the last two terms represent the homogeneous broadening due to exciton–phonon interactions. δ is the exciton–acoustic phonon coupling coefficient, Γ_{LO} represents the exciton longitudinal-optical (LO) phonon coupling coefficient, E_{LO} is the LO-phonon energy and K_B is the Boltzmann constant. The best-fit values for the experimental data were, $\Gamma_{inh} = 29$ meV, $\delta = 9.5$ $\mu\text{eV/K}$, $\Gamma_{LO} = 17$ meV, and $E_{LO} = 29.5$ meV. The extracted value for $\delta \sim 9.5$ $\mu\text{eV/K}$ is much less than the bulk CdSe value of 8 meV/K [45]. This indicates that the acoustic phonon coupling between the QDs and silica matrix is negligible as opposed to that of QDs embedded in organic matrices [46].

The scattering of the optical phonons, with the best-fit value of $\Gamma_{LO} = 17$ meV, is considerably reduced with respect to the bulk value of 100 meV [47], and this can be attributed to quantum confinement [48]. The best-fit value of the LO energy, $E_{LO} = 29.5$ meV, is slightly larger than the bulk value of 26.1 meV [43] and is not quite in agreement with the values expected from theory [49] and needs more investigation. Surface defects or trap states induced broadening could also have contributed to the homogeneous broadening [50].

B. Temperature-Dependent Excitonic Decay in QD/Silica Nanocrystals

To analyze the role of nonradiative processes on the relaxation dynamics of QD/silica NCs, the T -dependent excitonic decay in 77–300 K range was studied using TCSPC method. The raw decay data was deconvoluted from the IRF and distribution tail fitting analysis was performed, using an algorithm implemented in FAST software [see Fig. 6]. The fit quality was assured by criteria $\chi^2 < 1.3$, and the values of decay components extracted from the distribution analysis are shown in Table I. Due to the

TABLE I
DECAY COMPONENTS ACQUIRED FROM THE DISTRIBUTION TAIL FITTING ANALYSIS
FOR QD/SILICA NCs AT DIFFERENT TEMPERATURES

	$T = 77\text{K}$	$T = 117\text{K}$	$T = 157\text{K}$	$T = 197\text{K}$	$T = 237\text{K}$	$T = 277\text{K}$	$T = 300\text{K}$
τ_1 (ns)	0.50	0.50	0.50	0.50	–	0.50	0.50
τ_2 (ns)	9.35	6.64	6.65	6.80	5.96	3.30	3.15
τ_3 (ns)	42.21	13.98	14.65	18.02	21.36	11.24	–
τ_4 (ns)	327.6	81.06	56.18	74.96	73.06	–	–
B_1	0.57	10.06	11.01	5.72	–	39141.17	86828.98
B_2	1.10E5	3.70E5	4.10E5	5.20E5	1.50E6	6.60E8	1.70E9
B_3	17.13	20761.36	13340.7	5555.45	2486.64	24709.04	–
B_4	2.04	19.1	70.42	63.48	42.97	–	–
$\langle \tau \rangle$ (ns)	9.58	7.46	7.25	7.20	6.07	3.30	3.15
χ^2	0.93	1.14	1.29	1.37	1.37	0.89	0.8

T : temperature (K), τ : decay lifetime component (ns), B : pre-exponential factor, $\langle \tau \rangle$: average lifetime (ns), and χ^2 : fit quality indicator.

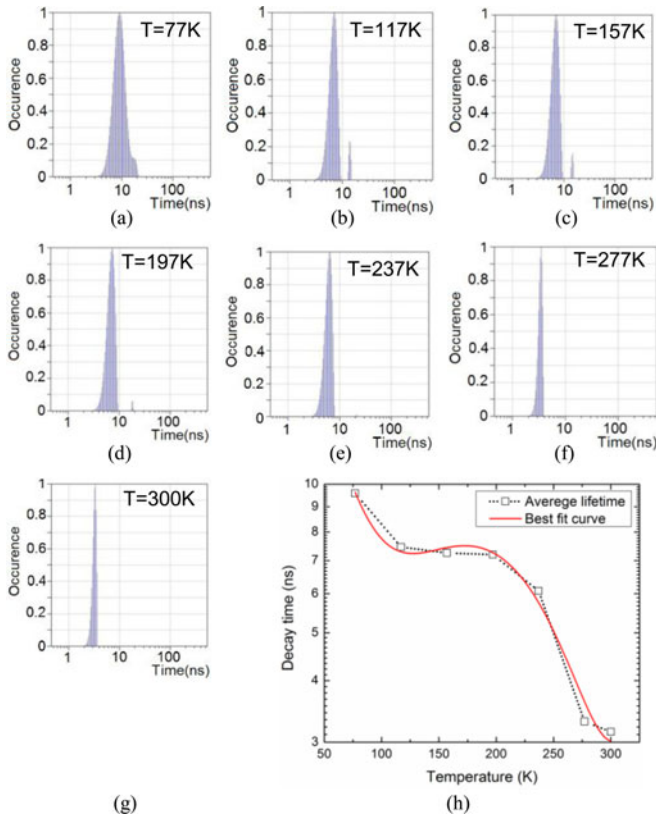


Fig. 7. Lifetime histograms obtained from distribution tail fitting analysis of QD/silica NCs at (a) 77 K, (b) 117 K, (c) 157 K, (d) 197 K, (e) 237 K, (f) 277 K, (g) 300 K, (h) PL decay as a function of temperature: experimental-empty rectangles/fit-red solid line.

limited instrument response, it was only possible to study the slow relaxation process. Up to four slow relaxation components with time constants in the nanosecond (ns) range were determined at each temperature. Table I also shows the average lifetime of the decay time constants calculated using the following [51]:

$$\langle \tau \rangle = \frac{B_1 \tau_1^2 + B_2 \tau_2^2 + B_3 \tau_3^2}{B_1 \tau_1 + B_2 \tau_2 + B_3 \tau_3}. \quad (3)$$

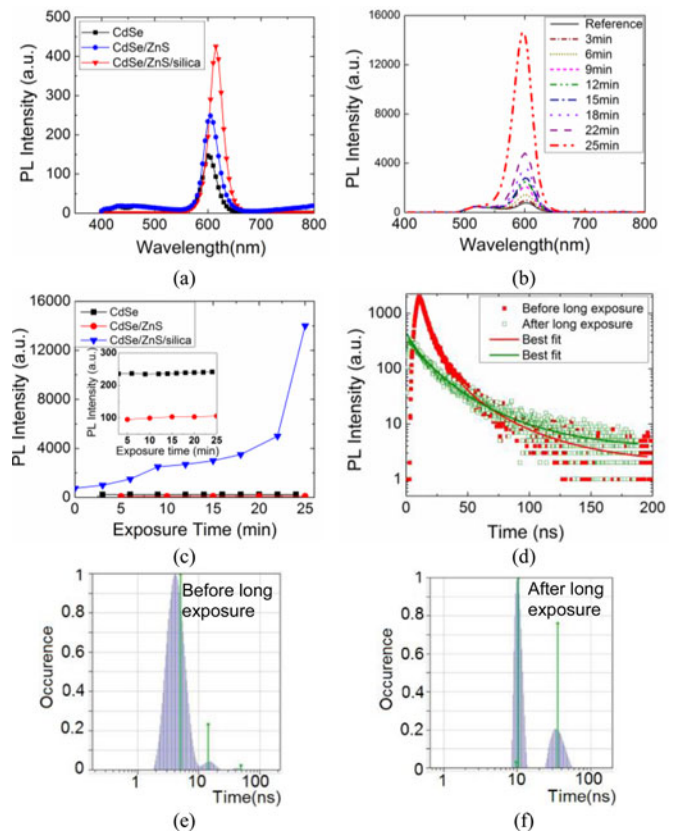


Fig. 8. (a) PL spectra of the core, core/shell QDs and (QD/silica) NCs. (b) PL spectra of QD/silica NCs after different illumination periods. (c) PL intensity after different illumination period for core, core/shell QDs (inset) and QD/silica NCs. (d) PL decay of QD/silica NCs before and after 25 min exposure. Lifetime histograms obtained from multiexponential (green lines) and distribution (Gaussian tails) tail fitting analyses for QD/silica NCs; (e) before and (f) after a long exposure.

The relaxation components point to the existence of a number of discrete relaxation pathways, each with an individual lifetime. The results show that the decay rate increases at higher temperatures.

The lifetime histograms, in Fig. 7(a)–(g), demonstrate that the decay time constants decrease at higher temperatures.

TABLE II
DECAY COMPONENTS ACQUIRED FROM THE MULTIEXPONENTIAL AND DISTRIBUTION TAIL FITTING ANALYSES FOR QD/SILICA NCs BEFORE AND AFTER A LONG EXPOSURE

Long exposure	Exponential Analyses				Distribution Analyses			
	B	τ (ns)	$\langle\tau\rangle$ (ns)	χ^2	B	τ (ns)	$\langle\tau\rangle$ (ns)	χ^2
Before	1719.19	4.89	13.10	1.29	16165.61	4.59	6.80	1.69
	392.00	13.99			1150.00	11.94		
	32.67	51.19			72.14	39.48		
After	3.34	9.52	27.83	1.34	305.05	10.44	24.60	1.75
	114.98	10.12			110.24	36.00		
	87.31	34.81			–	–		

Fig. 7(h) shows the average lifetime as a function of temperature. The average lifetime decreases slowly as the temperature increases from 77 K to 157 K followed by a slow increase in the 157–237 K range and finally a rapid decrease till 300 K. This behavior suggests the presence of more than one T -dependent nonradiative processes in the QD/silica NC ensemble. The decay in the 77 K–157 K range can be due to the size and shape inhomogeneities within the QD/silica NC ensemble [52] as a result of the Förster energy transfer between QDs [46]. In QD/silica NCs chemical transitions can take place on the surface due to the preparation technique so that the decay in low- T can also be due partly to the surface trap states. Slow decrease in the average lifetime of QD/silica NCs at low- T can be an indication of the ligand exchange during silica growth. However, ultrafast studies need to be done to further clarify the mechanism. In the 237–300 K range, the thermally activated process limiting the NC quantum efficiency can be attributed to the thermal escape from the QDs, assisted by scattering of LO phonons [53]. It can also be ascribed to thermally activated carrier trapping in surface and/or defect states at the ZnS/silica interface, attributed to the phase transition with ligand exchange during oxide growth [54].

The slight increase in the decay time in the mid- T ($157 < T < 273$) range can be related to the good passivation at the CdSe and ZnS interface or at the interface of ZnS and silica [55]. It should be noted that the surface-trapping process can be negligible at the CdSe/ZnS interface because of fairly good passivation with the ZnS shell, which can be seen from the PL spectra in Fig. 4.

C. Effect of Excitation and Exposure Periods on the PL Intensity and Decay Time of the QD/Silica Nanocrystals

Luminescence properties of the synthesized QD/silica NCs were compared to those of core (CdSe) and core/shell (CdSe/ZnS) QDs. Intense PL was observed for the QD/silica NCs, as shown in Fig. 8(a). This observation could be attributed to a slow exchange of organic ligands with hydrolyzed TEOS. In this paper, the TEOS hydrolysis with water alone is a very slow reaction, causing hydroxyl ligands to be orderly arranged on the QD surface and result in proper passivation of the surface [23], [33].

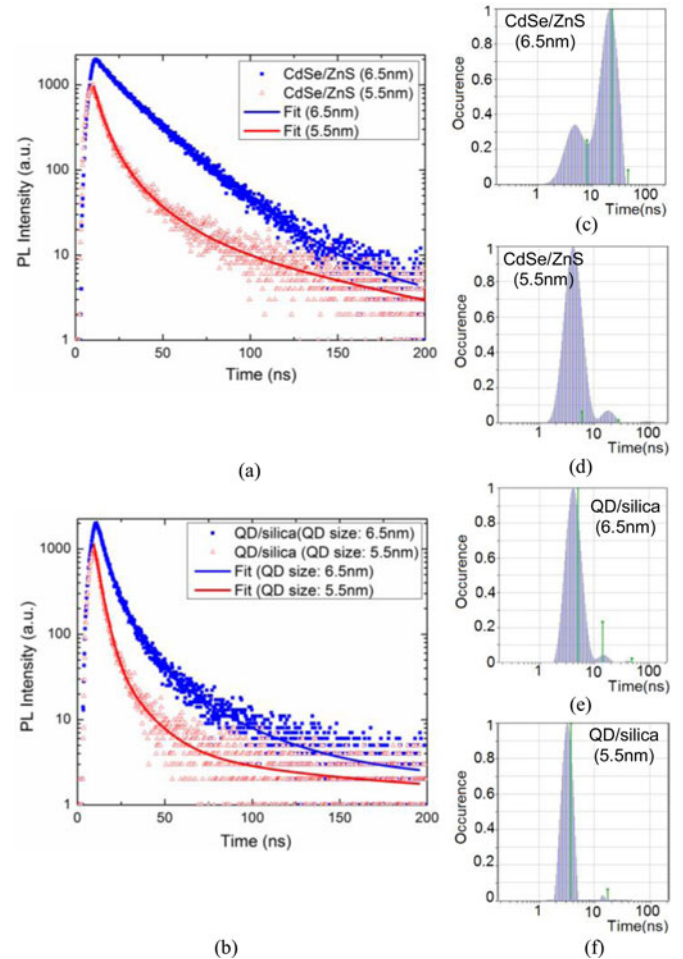


Fig. 9. Size-dependent energy relaxation in (a) CdSe/ZnS QDs, (b) QD/silica NCs. Lifetime histogram obtained by the multi-exponential (green lines) and distribution (Gaussian tails) tail fitting analyses for (c) 6.5 nm, (d) 5.5 nm CdSe/ZnS QDs and QD/silica NCs with (e) 6.5 nm, (f) 5.5 nm seed sizes.

The QD/silica NCs were also illuminated for different durations and significant improvement in PL was observed for the samples that were excited longer [see Fig. 8(b) and (c)]. Prolonged exposure resulted in steady blue shifts, revealing a slight blue shift of the exciton absorption and suggesting a photo-induced chemical change of the surface causing surface oxidation [56]. On the other hand, for both the CdSe and CdSe/ZnS QDs, the PL intensity only slightly changed after

TABLE III
DECAY COMPONENTS ACQUIRED FROM THE MULTIEXPONENTIAL AND DISTRIBUTION TAIL FITTING ANALYSES FOR DIFFERENT SIZES CdSe/ZnS QDs AND QD/SILICA NCs

QDs & QD/silica Different Sizes	Exponential Analyses				Distribution Analyses			
	B	τ (ns)	$\langle \tau \rangle$ (ns)	χ^2	B	τ (ns)	$\langle \tau \rangle$ (ns)	χ^2
CdSe/ZnS QDs 5.5 nm	13295.91	0.036	14.61	1.27	7304.34	4.4	11.52	1.52
	811.00	5.87			322.76	18.19		
	147.71	26.86			23.19	96.38		
CdSe/ZnS QDs 6.5 nm	382.08	7.755	23.61	1.62	1234.19	4.67	18.89	1.36
	1536.13	22.11			3579.03	20.04		
	119.10	42.85			–	–		
QD/silica 5.5 nm	1125.94	3.61	6.45	1.25	3.23	17329.77	4.18	1.63
	65.51	16.90			14.23	131.01		
	–	–			91.71	4.31		
QD/silica 6.5 nm	1713.32	4.88	12.73	1.29	20801.21	4.35	6.00	1.69
	394.67	13.79			507.33	15.03		
	35.87	47.72			51.98	42.45		

long exposure [inset of Fig. 8(c)]. Fig. 8(d) shows the PL decay lifetime of the QD/silica NCs before and after 25 min exposure. The corresponding lifetime histograms obtained from multiexponential and distribution tail fitting analyses are shown in Fig. 8(e) and (f).

The decay time constant components and the average lifetime are listed in Table II. The surface photo-oxidation produces a shell phase (ZnSO_4) on ZnS that improves surface passivation and further reduces nonradiative recombination rates [57], [58]. In addition to the photo-induced surface chemical change in the luminescent dots, the relative increase in the average PL decay lifetime can also be due to the long PL lifetime of the previously dark dots [59]. This behavior provides another indication to the ligand exchange in QDs during oxide growth.

D. Effect of QD Size on Excitonic Decay of QD/Silica Nanocrystals

Decay lifetime of the QDs and QD/silica NCs measured at room temperature show size-dependence. In Fig. 9(a) and (b), the measured decay lifetimes for CdSe/ZnS QDs and QD/silica NCs are compared for QD sizes of 6.5 and 5.5 nm. The time constants were obtained by the multiexponential and distribution tail fitting analyses. Corresponding lifetime histograms are shown in Fig. 9(c)–(f).

The decay components and average lifetimes are listed in Table III. The time constants and the average lifetime of the QDs follow the same size dependency as that of the QD/silica NCs. For instance, the average lifetime extracted from distribution tail fitting analyses decreased from 18.89 to 11.52 ns for the CdSe/ZnS QDs and from 6.00 to 4.18 ns for the QD/silica NCs, when the dot radius was reduced from 6.5 to 5.5 nm, indicating a decrease in decay time with decreasing size. Lifetimes extracted from multiexponential analyses also showed the same trend.

This behavior could be attributed to the pronounced surface transformation of smaller size QDs during the growth process that causes nonradiative energy transfers at surface states. It could be also due to the decay rates of bright and dark states that may have an effect on the decay lifetime of the NCs. In addition, an effective increase in the carrier concentrations resulting from

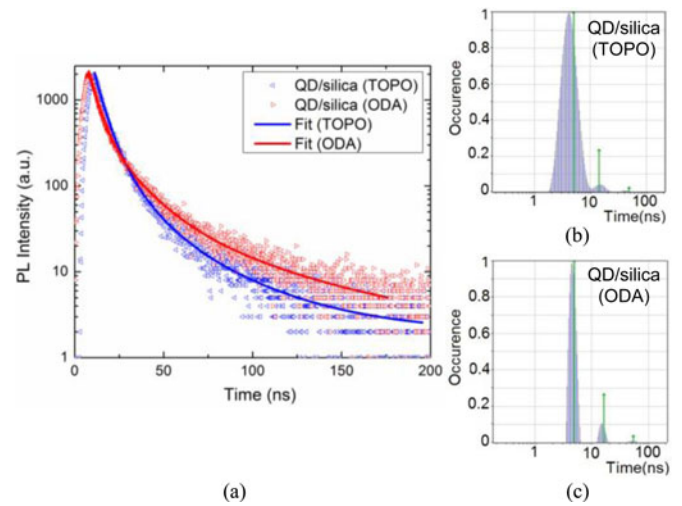


Fig. 10. (a) Excitonic decay of hydrophobically ligated QD/silica NCs; Lifetime histogram obtained by the multiexponential (green lines) and distribution (Gaussian tails) tail fitting analyses for (b) TOPO and (c) ODA ligated QD/silica NCs.

the increased spatial confinement [60] can be suggested as the enhancement in the decay rate in smaller particles.

Moreover, the average lifetime of the QD/silica NCs is less than the corresponding size QDs. This could be another indication of the exchange of QD ligand during oxide growth which results in surface chemical changes and causes the QD/silica NCs to experience nonradiative energy transfers. This effect is more profound for particles with smaller core sizes.

E. Effect of QD Ligand on Excitonic Decay of QD/Silica NCs

The decay dynamics of QD/silica NCs formed from two hydrophobically (ODA- and TOPO-) ligated QD seeds are compared as shown in Fig. 10(a). The time constants obtained from the multiexponential and distribution analyses indicate a low decay rate and accordingly improvement in lifetime of the ODA-ligated QD seeds (see Fig. 10(b), (c) and Table IV). From the results, it is predicted that the surface transition during silica growth affects the TOPO-stabilized QDs more than the

TABLE IV
DECAY COMPONENTS ACQUIRED FROM THE MULTIEXPONENTIAL AND DISTRIBUTION TAIL FITTING
ANALYSES FOR QD/SILICA NCS WITH TWO DIFFERENT HYDROPHOBIC LIGANDS

QD/silica Different Ligands	Exponential Analyses				Distribution Analyses			
	B	τ (ns)	$\langle \tau \rangle$ (ns)	χ^2	B	τ (ns)	$\langle \tau \rangle$ (ns)	χ^2
QD/silica-ODA	1723.83	4.75			8977.88	4.62		
	452.81	15.73	17.14	1.26	752.82	15.36	10.03	1.65
	58.49	53.07			70.69	53.26		
QD/silica-TOPO	1713.32	4.88			20801.21	4.35		
	394.67	13.79	12.73	1.29	507.33	15.03	6.00	1.69
	35.87	47.72			51.98	42.45		

ODA-stabilized QDs. This observation also supports ligand exchange as a possible mechanism for the silica growth.

VI. CONCLUSION

QD/silica NC structures have been formed using a microemulsion process using CdSe/ZnS core/shell QDs. The fabricated NCs have been structurally and optically characterized. Monodispersity in the growth process has been achieved. The relaxation dynamic studies on the QD/silica NCs suggest the interface carrier trapping and LO phonons scattering as the main nonradioactive relaxation processes. Results from the characterization and analyses suggested that ligand exchange to be the likeliest mechanism for the growth. Ligands used in the QD seeds as well as the size of the initial QDs influence the excitonic decay of the QD/silica NCs. The NCs displayed intense PL with a slight loss in LQE compared to the starting QDs. However, the results also showed that PL can be improved by prolonged illumination. From a device application point of view, this synthesis provides NCs containing QDs embedded in a transparent medium. Moreover, QD/silica NCs make the handling and deployment easy and safer compared to the core CdSe or CdSe/ZnS QDs. The resulting NCs can be further engineered to form layers for various LDS applications in the fields of photovoltaics, imaging, and detectors.

REFERENCES

- [1] D. Bera, L. Qian, T. Tseng, and P. Holloway, "Quantum dots and their multimodal applications: A review," *Materials*, vol. 3, pp. 2260–2345, 2010.
- [2] P. Bhattacharya, S. Ghosh, and A. Stiff-Roberts, "Quantum dot optoelectronic devices," *Annu. Rev. Mat. Res.*, vol. 34, pp. 1–40, 2004.
- [3] P. Prabhakaran, W. Kim, K. Lee, and P. Prasad, "Quantum dots (QDs) for photonic applications," *Opt. Mater. Exp.*, vol. 2, no. 5, pp. 578–593, 2012.
- [4] E. Klampaftis, D. Ross, K. McIntosh, and B. Richards, "Enhancing the performance of solar cells via luminescent down-shifting of the incident spectrum: A review," *Sol. Energ. Mat. Sol. C.*, vol. 93, pp. 1182–1194, 2009.
- [5] Z. Cheng, F. Su, L. Pan, M. Cao, and Z. Sun, "CdS quantum dot-embedded silica film as luminescent down-shifting layer for crystalline Si solar cells," *J. Alloy Compd.*, vol. 494, pp. L7–L10, 2010.
- [6] V. Sholin, J. Olson, and S. Carter, "Semiconducting polymers and quantum dots in luminescent solar concentrators for solar energy harvesting," *J. Appl. Phys.*, vol. 101, pp. 123114-1–123114-9, 2007.
- [7] E. Klampaftis, M. Congiu, N. Robertson, and B. Richards, "Luminescent ethylene vinyl acetate encapsulation layers for enhancing the short wavelength spectral response and efficiency of silicon photovoltaic modules," *IEEE J. Photovoltaics*, vol. 1, no. 1, pp. 29–36, Jul. 2011.
- [8] R. Nakata, N. Hashimoto, and K. Kawano, "High conversion efficiency solar cell using fluorescence of rare earth ions," *Jpn. J. Appl. Phys.*, vol. 35, pp. L90–L93, 1996.
- [9] P. Chung, H. Chung, and P. Holloway, "Phosphor coatings to enhance Si photovoltaic cell performance," *J. Vac. Sci. Technol. A*, vol. 25, pp. 61–66, 2007.
- [10] L. Danos, T. Parel, T. Markvart, V. Barrioz, W. Brooks, and S. Irvine, "Increased efficiencies on CdTe solar cells via luminescence down-shifting with excitation energy transfer between dyes," *Sol. Energ. Mat. Sol. C.*, vol. 98, pp. 486–490, 2012.
- [11] S. Geyer, J. Scherer, F. Jaworski, and M. Bawendi, "Multispectral imaging via luminescent down-shifting with colloidal quantum dots," *Opt. Mater. Exp.*, vol. 3, pp. 1167–1175, 2013.
- [12] S. Geyer, J. Scherer, M. Jack, M. Bawendi, and F. Jaworski, "Dual-band ultraviolet-short-wavelength infrared imaging via luminescent downshifting with colloidal quantum dots," *J. Nanophotonics*, vol. 7, pp. 073083-1–073083-9, 2013.
- [13] S. Coe-Sullivan, W. Liu, P. Allen, and J. Steckel, "Quantum dots for LED downconversion in display applications," *ECS J. Solid State Sci. Technol.*, vol. 2, pp. R3026–R3030, 2013.
- [14] S. Geyer, J. Scherer, N. Moloto, F. Jaworski, and M. Bawendi, "Efficient luminescent down-shifting detectors based on colloidal quantum dots for dual band detection applications," *ACS Nano*, vol. 5, no. 5, pp. 5566–5571, 2011.
- [15] J. De la Torre, G. Bremond, M. Lemiti, G. Guillot, P. Mur, and N. Buffet, "Using silicon nanostructures for the improvement of silicon solar cells' efficiency," *Thin Solid Films*, vols. 511/512, pp. 163–166, 2006.
- [16] B. Sadeghimakki and S. Sivoththaman, "Uniform embedment of CdSe/ZnS quantum dot arrays in thin oxide layers for luminescence down shifting in PV device," in *Proc. IEEE 35th Photovoltaic Spec. Conf.*, Hawaii, CA, USA, paper 978-1-4244-5892-9, 2010, pp. 002955–002959.
- [17] B. Sadeghimakki and S. Sivoththaman, "Investigation of structural and optical properties of CdSe quantum dots in glass matrices for photovoltaic application," *Proc. SPIE, Nanoscale Photonic Cell Tech. for PVs*, vol. 7047, pp. 7047W-1–7047W-9, 2008.
- [18] S. Maenosono, T. Okubo, and Y. Yamaguchi, "Overview of nanoparticle array formation by wet coating," *J. Nanopart. Res.*, vol. 5, pp. 5–15, 2003.
- [19] G. Alombert-Goget, C. Armellini, S. Berneschi, B. Boulard, A. Chiappini, A. Chiasera, C. Duverger-Arfuso, P. Féron, M. Ferrari, S. Guddala, E. Moser, S. Pelli, D. N. Rao, G. C. Righini, and G. Speranza, "Fabrication, assessment, and application of confined structures in photonic glasses," in *Proc. Third ICTON Mediterranean Winter Conf.*, Angers, France, paper Fr1.1, 2009, pp. 1–6.
- [20] C. Graf and A. van Blaaderen, "Metallo-dielectric colloidal core-shell particles for photonic application," *Langmuir*, vol. 18, pp. 524–534, 2002.
- [21] Y. Jin and X. Gao, "Plasmonic fluorescent quantum dots," *Nature Nanotech.*, vol. 4, pp. 571–576, 2009.
- [22] J. L. Pelley, A. S. Daar, and M. A. Saner, "State of academic knowledge on toxicity and biological fate of quantum dots," *Toxicol. Sci.*, vol. 112, no. 2, pp. 276–296, 2009.
- [23] M. Darbandi, R. Thomann, and T. Nann, "Single quantum dots in silica spheres by microemulsion synthesis," *Chem. Mater.*, vol. 17, no. 23, pp. 5720–5725, 2005.

- [24] B. Dubertret, P. Skourides, D. Norris, V. Noireaux, A. Brivanlou, and A. Libchaber, "In vivo imaging of quantum dots encapsulated in phospholipid micelles," *Science*, vol. 298, pp. 1759–1762, 2002.
- [25] B. Sadeghimakki, N. M. S. Jahed, and S. Sivoththaman, "Photoluminescence properties of core/shell CdSe/ZnS quantum dots embedded in transparent films for third generation photovoltaics," in *Proc. Mater. Res. Soc. Symp.*, 2011, vol. 1322, pp. 39–44.
- [26] W.-S. Song, J.-H. Kim, and H. Yang, "Silica-embedded quantum dots as downconverters of light-emitting diode and effect of silica on device operational stability," *Mater. Lett.*, vol. 111, pp. 104–107, 2013.
- [27] J.-C. Hsu, C.-C. Huang, K.-L. Ou, N. Lu, F.-D. Mai, J.-K. Chen, and J.-Y. Chang, "Silica nanohybrids integrated with CuInS₂/ZnS quantum dots and magnetite nanocrystals: Multifunctional agents for dual-modality imaging and drug delivery," *J. Mater. Chem.*, vol. 21, pp. 19257–19266, 2011.
- [28] W. Stöber, A. Fink, and E. Bohn, "Controlled growth of monodisperse silica spheres in the micron size range," *J. Colloid Interface Sci.*, vol. 26, pp. 62–69, 1968.
- [29] D. K. Yi, S. T. Selvan, S. S. Lee, G. C. Papaefthymiou, D. Kundaliya, and J. Y. Ying, "Silica-coated nanocomposites of magnetic nanoparticles and quantum dots," *J. Amer. Chem. Soc.*, vol. 127, pp. 4990–4991, 2005.
- [30] K. Osseo-Asare and F. J. Arriagada, "Preparation of SiO₂ nanoparticles in a non-ionic reverse micellar system," *Colloids Surf.*, vol. 50, pp. 321–339, 1990.
- [31] H. Kim, H. S. Jang, B.-H. Kwon, M. Suh, Y. Kim, S. H. Cheong, and D. Y. Jeona, "In situ synthesis of thiol-capped CuInS₂-ZnS quantum dots embedded in silica powder by sequential ligand-exchange and silanization," *Electrochem. Solid-State Lett.*, vol. 15, no. 2, pp. K16–K18, 2012.
- [32] H. Kim, M. Suh, B. Kwon, D. S. Jang, S. W. Kim, and D. Y. Jeon, "In situ ligand exchange of thiol-capped CuInS₂/ZnS quantum dots at growth stage without affecting luminescent characteristics," *J. Colloid Interface Sci.*, vol. 363, pp. 703–706, 2011.
- [33] P. Yang, M. Ando, and N. Murase, "Highly luminescent CdSe/Cd_xZn_{1-x}S quantum dots coated with thickness-controlled SiO₂ shell through silanization," *Langmuir*, vol. 27, pp. 9535–9540, 2011.
- [34] R. Koole, M. M. van Schooneveld, J. Hilhorst, C. M. Donega, D. C. Hart, A. van Blassderen, D. Vandmackelbergh, and A. Meijerink, "On the incorporation mechanism of hydrophobic quantum dots in silica spheres by a reverse microemulsion method," *Chem. Mater.*, vol. 20, pp. 2503–2512, 2008.
- [35] M. R. Linford and C. E. D. Chidsey, "Alkyl monolayers covalently bonded to silicon surfaces," *J. Amer. Chem. Soc.*, vol. 115, pp. 12631–12632, 1993.
- [36] P. L. Llewellyn, S. Bourrelly, C. Serre, A. Vimont, M. Daturi, L. Hamon, G. D. Weireld, J.-S. Chang, D.-Y. Hong, Y. K. Hwang, S. H. Jung, and G. Férey, "High uptakes of CO₂ and CH₄ in mesoporous metal-organic frameworks MIL-100 and MIL-101," *Langmuir*, vol. 24, pp. 7245–7250, 2008.
- [37] S. Y. Venyaminov and F. G. Prendergast, "Water (H₂O and D₂O) molar absorptivity in the 1000–4000 cm⁻¹ range and quantitative infrared spectroscopy of aqueous solutions," *Anal. Biochem.*, vol. 248, pp. 234–245, 1997.
- [38] F. Dousseau, M. Therrien, and M. Pérzolet, "On the spectral subtraction of water from the FT-IR spectra of aqueous solutions of proteins," *Appl. Spectrosc.*, vol. 43, no. 3, pp. 538–542, 1989.
- [39] P. A. Connor, K. D. Dobson, and A. J. McQuillan, "Infrared spectroscopy of the TiO₂/aqueous solution interface," *Langmuir*, vol. 15, pp. 2402–2408, 1999.
- [40] P. Innocenzi, "Infrared spectroscopy of sol-gel derived silica-based films: A spectra-microstructure overview," *J. Non-Cryst. Solids*, vol. 316, pp. 309–319, 2003.
- [41] L. Lefort, M. Chabanas, O. Maury, D. Meunier, C. Copérret, J. Thivolle-Cazat, and J.-M. Basset, "Versatility of silica used as a ligand: Effect of thermal treatments of silica on the nature of silica-supported alkyl tantalum species," *J. Organomet. Chem.*, vols. 593/594, pp. 96–100, 2000.
- [42] Y. P. Varshni, "Temperature dependence of the energy gap in semiconductors," *Physica (Amsterdam)*, vol. 34, no. 1, pp. 149–154, 1967.
- [43] L. Landolt, R. Börnstein, K. H. Hellwege, W. Freyland, M. Schulz, H. Weiss, and Landolt-Börnstein, *Numerical Data and Functional Relationship in Science and Technology*, New Series, Group III, Berlin, Germany: Springer-Verlag, 1982, vol. 17, Pt. B.
- [44] L. G. Zhang, D. Z. Shen, X. W. Fan, and S. Z. Lu, "Exciton-phonon scattering in CdSe/ZnSe quantum dots," *Chin. Phys. Lett.*, vol. 19, no. 4, pp. 578–580, 2002.
- [45] F. Gindele, K. Hild, W. Langbein, and U. Woggon, "Temperature-dependent line widths of single excitons and biexcitons," *J. Lumin.*, vols. 87–89, pp. 381–383, 2000.
- [46] D. Valerini, A. Cretí, and M. Lomascolo, "Temperature dependence of the photoluminescence properties of colloidal CdSe/ZnS core/shell quantum dots embedded in a polystyrene matrix," *Phys. Rev. B*, vol. 71, pp. 235409-1–235409-6, 2005.
- [47] J. Voigt, F. Spielgelberg, and M. Senoner, "Band parameters of CdS and CdSe single crystals determined from optical exciton spectra," *Phys. Status Solidi B*, vol. 91, no. 1, pp. 189–199, 1979.
- [48] S. Nomura and T. Kobayashi, "Exciton-LO-phonon couplings in spherical semiconductor microcrystallites," *Phys. Rev. B*, vol. 45, pp. 1305–1316, 1992.
- [49] C. Trallero-Giner, A. Debernardi, M. Cardona, E. MenendezProupin, and A. I. Ekimov, "Optical vibrons in CdSe dots and dispersion relation of the bulk material," *Phys. Rev. B*, vol. 57, pp. 4664–4669, 1998.
- [50] T. Takagahara, "Electron-phonon interactions in semiconductor nanocrystals," *J. Lumin.*, vol. 70, nos. 1–6, pp. 129–143, 1996.
- [51] A. Kongkanand, K. Tvrđy, K. Takechi, M. Kuno, and P. V. Kamat, "Quantum dot solar cells. Tuning photoresponse through size and shape control of CdSe-TiO₂ architecture," *J. Amer. Chem. Soc.*, vol. 130, no. 12, pp. 4007–4015, 2008.
- [52] C. de Mello Donegá, M. Bode, and A. Meijerink, "Size- and temperature-dependence of exciton lifetimes in CdSe quantum dots," *Phys. Rev. B*, vol. 74, pp. 085320-1–085320-9, 2006.
- [53] Y. N. Hwang, S. H. Park, and D. Kim, "Size-dependent surface phonon mode of CdSe quantum dots," *Phys. Rev. B*, vol. 59, pp. 7285–7288, 1999.
- [54] S. A. Crooker, T. Barrick, J. A. Hollingsworth, and V. I. Klimov, "Multiple temperature regimes of radiative decay in CdSe nanocrystal quantum dots: Intrinsic limits to the dark-exciton lifetime," *Appl. Phys. Lett.*, vol. 82, pp. 2793–2795, 2003.
- [55] M. Hong, M. Guo-Hong, W. Wen-Jun, G. Xue-Xi, and M. Hong-Liang, "Size-dependent optical properties and carriers dynamics in CdSe/ZnS quantum dots," *Chin. Phys. B*, vol. 17, no. 4, pp. 1280–1284, Apr. 2008.
- [56] S. Dembski, C. Graf, T. Krüger, U. Gbureck, A. Ewald, A. Bock, and E. Rühl, "Photoactivation of CdSe/ZnS quantum dots embedded in silica colloids," *Small*, vol. 4, no. 9, pp. 1516–1526, 2008.
- [57] E.-P. Jang, W.-S. Song, K.-H. Lee, and H. Yang, "Preparation of a photo-degradation resistant quantum dot-polymer composite plate for use in the fabrication of a high-stability white-light-emitting diode," *Nanotechnology*, vol. 24, pp. 045607-1–045607-9, 2013.
- [58] H. Yang and P. H. Holloway, "CdS: Mn nanocrystals passivated by ZnS: Synthesis and luminescent properties," *J. Chem. Phys.*, vol. 121, no. 20, pp. 10233–10240, 2004.
- [59] Y. Ebenstein, T. Mokari, and U. Banin, "Fluorescence quantum yield of CdSe/ZnS nanocrystals investigated by correlated atomic-force and single-particle fluorescence microscopy," *Appl. Phys. Lett.*, vol. 80, no. 21, pp. 4033–4035, 2002.
- [60] V. I. Klimov, A. A. Mikhailovsky, D. W. McBranch, C. A. Leatherdale, and M. G. Bawendi, "Quantization of multiparticle Auger rates in semiconductor quantum dots," *Science*, vol. 282, no. 5455, pp. 1011–1013, 2000.



Bahareh Sadeghimakki (S'10–M'13) received the B.S. and M.S. degrees in physics from the Shahid Beheshti University, Iran, in 1999 and K. N. T. University of Technology, Iran, in 2003, respectively, and the Ph.D. degree in electrical and computer engineering from the University of Waterloo, ON, Canada, in 2012.

Since then she has been a Postdoctoral Fellow at the Department of Electrical and Computer Engineering. Her current research interests include semiconductor devices, next generation photovoltaic and

light emitting devices, microelectronics and nanofabrication.



Navid M. S. Jahed (S'10) received the B.S. and M.S. degrees in electrical engineering from the University of Tabriz, Iran, in 2007 and Sharif University of Technology, Iran, in 2009, respectively. He is currently working toward the Ph.D. degree at the Department of Electrical and Computer Engineering, University of Waterloo, ON, Canada.

His current research interests include next generation photovoltaics, and quantum dot and nanowire-based photovoltaic technologies.



Siva Sivoththaman (S'84–M'93–SM'98) received the Ph.D. degree from the University of Paris, France, in 1993.

He is currently a Professor at the Department of Electrical and Computer Engineering, University of Waterloo, Canada. He has published more than 150 journal and conference papers. He currently holds the Ontario Research Chair in Renewable Energy Technologies and Health, and is also the Director of the Centre for Advanced Photovoltaic Devices and Systems. He held the NSERC Industrial Research Associate Chair in RF-MEMS in 2002–2006. His current research interests include photovoltaics, microelectronics, MEMS, nanotechnologies, and health and safety of renewable energy technologies.